Indian Geotech J (October–December 2015) 45(4):431–440
DOI 10.1007/s40098-015-0164-4

ORIGINAL PAPER

# Detecting Gilgai Relief Beneath Sealed Flexible Pavements Using Road Profile and Road Roughness Measurements

**Robert P. Evans**[1] · **Arul Arulrajah**[1] · **Suksun Horpibulsuk**[1,2]

Received: 13 May 2015 / Accepted: 16 August 2015 / Published online: 29 August 2015


**Abstract** Expansive soils are those that expand and contract significantly when subjected to changes in moisture. The presence of such soils can accelerate the deterioration rate of pavements due to increased cracking and roughness, especially when Gilgai relief is allowed to manifest beneath the pavement structure. Gilgai relief is a naturally occurring topographical feature that results in a unique undulating ground surface. These undulations develop from deep seated swelling pressures within the underlying expansive soil layers. At present, current road roughness indices cannot isolate the roughness caused by Gilgai relief and the detection of Gilgai in the field can be difficult. This paper presents a new series of templates that can identify pavement sections that contain high concentrations of waveband roughness specific to Gilgai characteristics. These templates are based on the standard international roughness index and a variety of new calculated profile indices that measure waveband roughness quantities. The main outcome of this paper is that the influence of Gilgai relief can now be detected and quantified mathematically through these templates, which were developed from over 600 km of road profile data from flexible rural highway pavements located in north-west Victoria (Australia).

**Keywords** Expansive soil · Gilgai · Road roughness · Waveband analysis

✉ Robert P. Evans
robertevans@swin.edu.au

Arul Arulrajah
aarulrajah@swin.edu.au

Suksun Horpibulsuk
suksun@g.sut.ac.th

[1] Faculty of Science, Engineering and Technology, Swinburne University of Technology, P. O. Box 218, Hawthorn, VIC 3122, Australia

[2] School of Civil Engineering, Suranaree University of Technology, Nakhon Ratchasima 30000, Thailand

## Introduction

Expansive soils are those that expand and contract (i.e. swell and shrink) significantly when subjected to changes in moisture. The presence of an expansive subgrade beneath a pavement structure can cause significant deterioration problems, such as increased cracking and roughness. Site factors such as climate, site topography (drainage) and the presence of roadside vegetation have all shown to influence ground moisture conditions, and thus have a direct influence on the potential damaging effect of an expansive subgrade [1–5]. Longitudinal cracking in the outer wheel path is a clear indicator of a shrinking subgrade. This cracking primarily occurs due to natural drying of the soil beneath the edge of the pavement. As the soil dries, it contracts and succumbs to tensile failure (i.e. cracks) [6]. These cracks then reflect up through the pavement base material and present in the seal. As for roughness, this typically results from swelling within the expansive subgrade. If shrinkage cracks in the soil adjacent to the pavement are wide and deep enough to carry water deep into the expansive subgrade, this will promote a rapid local deep seated swelling pressure. This action is responsible for the initial development of Gilgai relief [7, 8].

Gilgai relief is essentially a topographical feature that manifests in expansive soil deposits that result in a unique undulating surface terrain. Gilgai phenomenon was first reported in Australia by Aitchison [9] and has since been investigated and reported widely by others [10–13]. The

Australian Handbook of Soils [13] best describes Gilgai phenomenon as a soil that is in a state of slow continuous movement in which soil from the deeper layers is brought to the surface on the mounds, and soil from the surface slips down to lower levels in the holes and cracks of the depressions. This publication also identified and labelled various mature structural forms of Gilgai as Normal, Melon-hole, Stony, Lattice, Wavy and Tank Gilgai. Each form is largely dependent upon the initial topography, rainfall patterns and thickness of expansive soil layers present. The term Gilgai originated in Australia as Aboriginal people use it to describe a small water hole. This is an accurate descriptor for the phenomenon as water often ponds in the depressions between the Gilgai mounds during the wetter months. Many published aerial photographs of mature Gilgai fields have clearly captured this effect [8, 10, 11], which is particularly true for the recorded Gilgai fields in Queensland (Australia) and Texas (USA).

In Australia, approximately 20 % of its area is covered by moderately to highly expansive soils [2]. A considerable amount of this expansive soil is located where the climate is conducive to the development of Gilgai relief. The distribution of potential Gilgai relief in Australia has been mapped and is presented in Fig. 1 [14]. The inset in Fig. 1 details the location of alluvial grey cracking clay deposits (in dark orange, covering the townships of Horsham, Warracknabeal and Litchfield) that are notorious for developing Gilgai relief and is the location of the test sites. Throughout Australia, the series of undulations that make up the Gilgai relief have been recorded to range in length from 4 to 40 m with an amplitude from a couple of centimetres up to 2 m. In Victoria (south-east region of Australia), Gilgai relief is typically not as well developed with amplitudes recorded only to 0.34 m [10, 15–17]. Nevertheless, these undulations are enough to cause significant problems to pavements and road users in these areas.

## Road Roughness

The international roughness index (IRI) is the most common road profile roughness index used throughout the world today. It was developed from data collected during the international road roughness experiment in 1982, which was funded by the World Bank [18, 19]. The IRI that resulted was based on a clearly defined mathematical "quarter-car" model that simulated a traditional response type road roughness measuring system (from a measured longitudinal road profile). The model is influenced by sprung and unsprung masses, springs and damping parameters of a passenger vehicle travelling at 80 km/h. Details on the calculation of the IRI have been well documented elsewhere [20, 21]. The primary reason for developing the IRI was to provide road agencies with a stable and repeatable roughness index that could be transportable between agencies. The response of the quarter-car filter used to calculate the IRI is shown in Fig. 2 [22]. It theoretically responds to wavelengths from 0.5 to 100 m but is largely influenced by wavelengths between 1.2 and 30 m, where the gain for profile slope is >0.5. Furthermore, the IRI quarter-car filter is most sensitive at wavelengths 2.4 and 15.4 m (i.e. wave numbers 0.065 and 0.42 cycles/m). These wavelengths are considered most likely to cause axle hop and body bounce in passenger type vehicles, which produces maximum passenger discomfort. However, heavy commercial vehicles respond very different to passenger cars where most discomfort comes from roughness in the longer wavelengths [23].

As Gilgai relief has been shown to produce undulations with wavelengths ranging from 4 to 40 m, pavement roughness caused by Gilgai relief is being only partially captured through the IRI. This is due to the quarter-car filter averaging the roughness data over a large bandwidth and favouring two distinct wavelengths (i.e. 2.4 and 15.4 m). For example, based on the response of the quarter-car filter (Fig. 2) the gain for profile slope is equal to a magnitude of 1.25 and 0.25 at wavelengths 4 and 40 m respectively. This is a significant variation and is much lower than the filter's maximum gain of 1.6 at wavelength 2.4 m. It is for this reason that the IRI is incapable of detecting the concentration or quantity of roughness generated by Gilgai relief (i.e. roughness at particular wavelengths). Thus, individual waveband indices are warranted to accurately measure quantities of such specific waveband roughness.

## Waveband Analysis

Waveband analysis can be performed by simply filtering longitudinal road profile data using either: (1) Butterworth filter, (2) Power spectral density (PSD) analysis, (3) Wavelet analysis, and (4) Application of the Hilbert–Huang transform. However, this paper will only report on the Butterworth filter and PSD analysis.

### Butterworth Filter

The Butterworth filter is a general band pass filter with low and high spatial cut off frequencies (or wave numbers), which are defined where the filter gain equals $1/\sqrt{2}$ (or 0.7071). The Butterworth filter was designed by Stephen Butterworth in 1930 to specifically have a frequency response as smooth and flat as mathematically possible in the pass band [24]. It was for this reason that the Butterworth filter was included in the RoadRuf software package

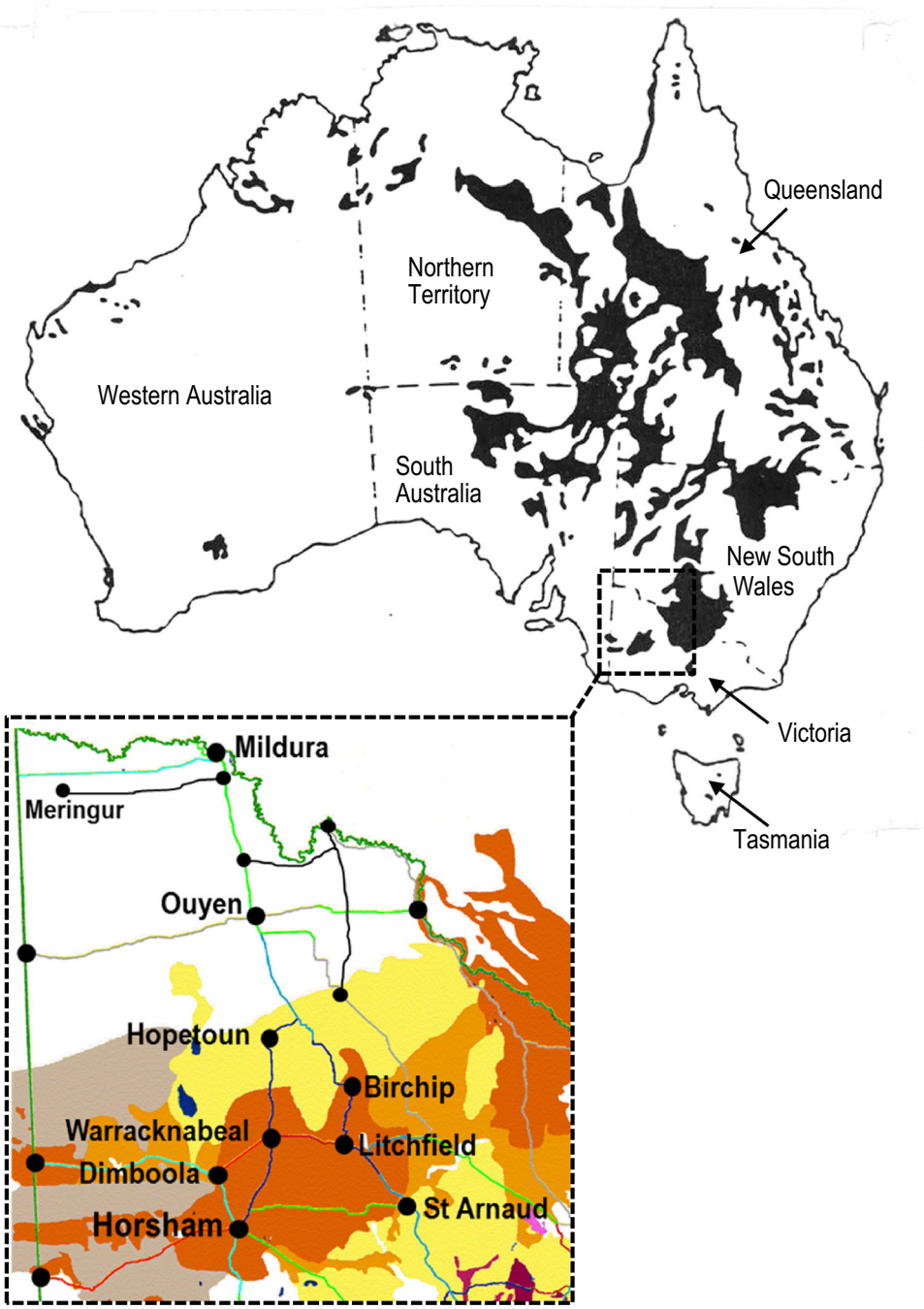


**Fig. 1** Distribution of potential Gilgai relief throughout Australia including a locality insert identifying the pavement test sites versus geological group [14, 26 Chpt 2]

for analysing and filtering longitudinal road profiles [25]. The theoretical transfer function and frequency response of the Four Pole Butterworth band pass filter has been best presented by Sayers and Karamihas [22].

A profile index or summary index can be computed from the Butterworth filtered profile using Eq. (1). This equation is identical to that used to calculate the IRI profile index from the quarter-car filtered profile. It can be set up to calculate average rectified values (mean absolute values) such as the IRI as well as root mean square values. For average rectified values, the adjustable accumulator exponent (P) must equal one and for root mean square values, P must equal two.

$$PI = \left(\frac{1}{N}\sum^{N}|F(x)|^{P}\right)^{\frac{1}{P}} \quad (1)$$

where $PI$ profile or summary index (m/km), $N$ number of points in the filtered profile, $F(x)$ filtered profile, $P$ adjustable accumulator exponent.

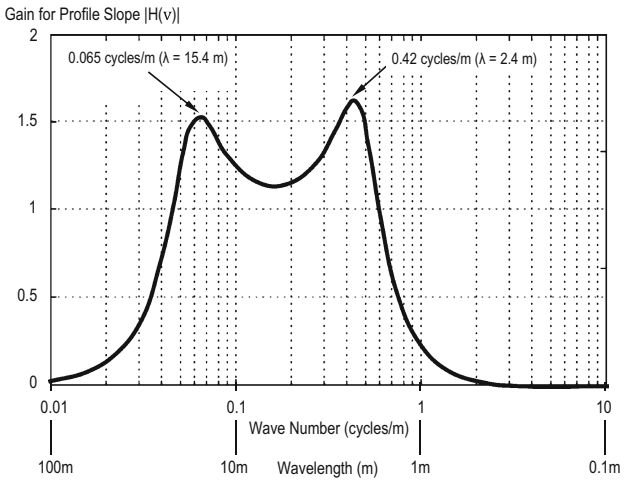


**Fig. 2** Wavenumber response of the IRI quarter-car filter [22]

## Power Spectral Density Analysis

Power spectral density (PSD) analysis originated in the field of Electrical Engineering, where the Fourier Transform was applied to voltages in order to illustrate the distribution of electrical power over frequency. The same mathematical calculations have since been applied to road profiles to evaluate the distribution of roughness over wave number (spatial frequency). In brief, the Fourier transform is used to compute amplitudes of sinusoids to construct the longitudinal road profile (elevation versus distance). As an equation for the non-periodic road profile is unknown, the Fourier transform uses the road profile sample points to decompose it into a series of sinusoidal functions with discrete frequencies (wave numbers). As multiple sinusoids are required to build a complex road profile, individual amplitudes are often very small. PSD analysis is essentially a scaled Fourier transform to show how the variance of the road profile is distributed over a set of sinusoids, or more commonly known as wave numbers [22]. A typical PSD of slope versus wave number plot is shown in Fig. 3 [26, Chpt 2]. The two lines (red with triangular markers and black with circular markers) actually represent the same section of pavement. One profile was recorded in 2005 before the pavement was rehabilitated and the other recorded just after in 2007. The effect of rehabilitation or change in condition of the pavement is clearly visible, especially for the waveband interval of 0.06–3 cycles/m (i.e. $\lambda = 0.33$–$16.7$ m). By converting the profile to slope, the resulting PSD of slope versus wave number plot is usually confined to within only one or two orders of magnitude [22]. Consequently, this increases the vertical scale and reveals the spectral properties in greater detail.

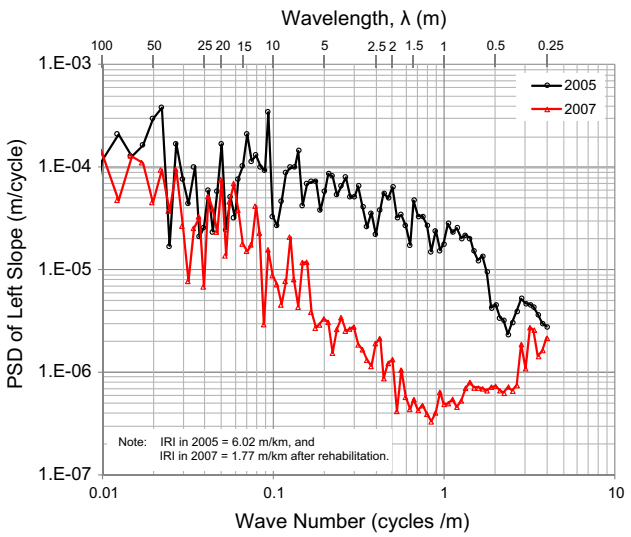


**Fig. 3** Typical plot of PSD of profile slope versus wave number (and wavelength) for a pavement before and after maintenance [26, Chpt 2]

As the area under the PSD versus wave number plot is equal to the mean square or variance of the road profile, the root of the area under the same plot is defined as the root mean square (RMS) summary statistic of the profile [27]. Furthermore, this RMS summary statistic of the road profile can be weighted to essentially act as a band pass filter in order to evaluate independent wavebands.

Although the PSD analysis technique does offer many advantages when analysing road profiles, it also has some disadvantages or limitations. These include: (1) PSD analysis via the Fourier Transform works best for repeating periodic signals, or stationary data. As road profile data is complex and definitely non-stationary by nature, the PSD analysis would be unable to detect all the wavebands with a high degree of statistical accuracy. (2) PSD analysis, like the IRI, only provides a summary statistic per section of pavement (typically every 100 m in Australia). Therefore, PSD indices would still not be able to reveal the specific location of pavement distress. It can only provide an approximate location dependent on the reporting interval. (3) Current literature encourages that the minimum length of any data signal (i.e. road longitudinal profile) analysed by PSD should be at least ten times the length of the waveband being investigated [28]. For example, a 300 m long road profile would be required to successfully capture enough detail to confidently report a weighted RMS statistic using a waveband whose centre wavelength is 30 m. This exacerbates the previous item as this may increase the reporting interval of the PSD summary statistics to greater than 100 m for the longer wavelengths.

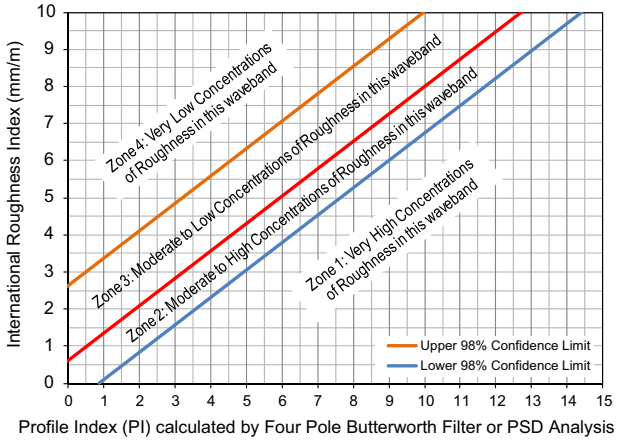


**Fig. 4** A generic example of a waveband identification template used to detect pavements with high concentrations of waveband roughness

## Identification of Long Wavelength Roughness Concentrations (Gilgai Relief) Using Newly Developed Templates

A series of new templates have been developed and are presented in this paper. These templates essentially identify pavement sections that contain abnormally high concentrations of specific waveband roughness, particularly for pavement sections suffering from long wavelength roughness (i.e. Gilgai relief). By identifying the dominant roughness wavebands present within a pavement, better pavement deterioration analysis should be achievable and allow more appropriate (and more effective) maintenance strategies to be employed.

It was decided to incorporate the IRI into these new templates due to its global acceptance amongst pavement engineers and road asset managers. Preservation of the well understood IRI scale was seen as an advantage as it was expected to assist with the perception of waveband roughness limits.

In developing these new templates, various waveband roughness indices were created, calculated and plotted against IRI for over 640 km of sealed flexible highway pavement. All pavement sections were located in the far north-west region of Victoria (Australia) where climatic conditions are similar and the geology is stable, which comprises largely alluvial silts and sands with minimum reactive qualities. This region is represented in Fig. 1 (inset) by the white colour—covering the townships of Ouyen, Hattah, Mildura and Meringur. It was expected that these sites would reveal a typical or normal distribution of waveband roughness concentrations for each of the wavebands investigated. A generic template is presented in Fig. 4, which clearly illustrates the nature of the template and the four distinct zones [26, Chpt 5]. In forming the boundaries within each template, upper and lower confidence limits were set at 98 % and established in the form of regression equations. This produced a 96 percentile confidence zone that was expected to represent normal waveband roughness concentrations for each of the waveband profile indices investigated. Therefore, zone 1 on the template is defined as the area beneath the 98 percentile lower confidence limit equation and indicates that very high concentrations of roughness are present in the pavement for that specific waveband. Alternately, zone 4 is the area above the 98 percentile upper confidence limit equation and indicates that very low concentrations of roughness have been detected. Consequently, zones 2 and 3 indicate that moderate (or expected) concentrations of waveband roughness have been detected in the pavement.

The waveband roughness indices investigated were split into single, double and triple octave bandwidths and were calculated from the raw longitudinal wheel path profile

**Fig. 5** Wavelength boundaries for the single, double and triple octave wavebands investigated

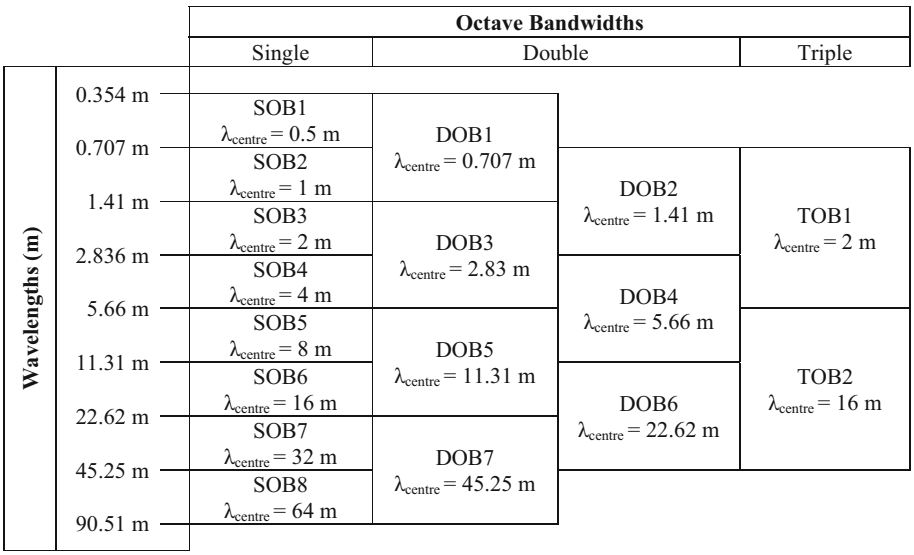

data. A graphical representation of the bandwidths used to separate each waveband is shown in Fig. 5. As an example, SOB5 represents Single Octave Band No. 5 with lower and upper wavelength boundaries of 5.66 and 11.31 m respectively. Indices that were expected to best detect Gilgai relief were those that measure the wavelength roughness between 4 and 30 m (i.e. SOB4–SOB7, DOB4–DOB6 and TOB2). All profile indices were calculated using the RoadRuf software [25] using weighted mean absolute value indices and root mean square indices.

In developing these waveband identification templates, linear regression equations produced the best correlation between IRI and individual waveband profile index using the Butterworth filter and PSD analysis. Table 1 lists some of these linear regression equations for the Butterworth filter based on 100 m profile lengths, which allow individual templates to be constructed for each single, double and triple octave waveband. Coefficient of determination ($R^2$) correlation values are also listed for each of the average regression equations, which were based on 6278 data points from over 640 km of pavement. Other linear regression equations for the Butterworth (RMS) indices and PSD indices can be found in the author's dissertation [26, Chpt 5]. Although these regression equations have been developed using a set of flexible pavements in Australia, the waveband profile indices and method can be used to build sets of templates to suit different geographical regions.

## Mapping Waveband Roughness Concentrations and Detecting the Presence of Gilgai Relief

To evaluate these new templates (described in the previous section), rural highway pavements surrounding the townships of Horsham, Warracknabeal and Litchfield were selected. These sites are shown in dark orange in the inset of Fig. 1 and comprise of alluvial grey cracking clay deposits that are highly susceptible to the development of Gilgai relief undulations. It was expected that these pavements would reveal a greater frequency of sections displaying abnormally high concentrations of long wavelength roughness (i.e. a greater frequency zone 1 results on the relevant long wavelength template).

**Table 1** Recommended lower, average and upper linear regression equations for the Butterworth (mean absolute value) profile index templates [26, Chpt 5]

| Waveband | Linear regression equations | | $R^2$ |
|---|---|---|---|
| Single, double and triple octaves | | | |
| SOB4: $\lambda$ = 2.828–5.657 m | Upper | $IRI = 2.36\ PI_{SOB4} + 0.69$ | 0.95 |
| | Average | $IRI = 2.36\ PI_{SOB4} + 0.15$ | |
| | Lower | $IRI = 2.36\ PI_{SOB4} - 0.19$ | |
| SOB5: $\lambda$ = 5.657–11.31 m | Upper | $IRI = 2.47\ PI_{SOB5} + 1.29$ | 0.90 |
| | Average | $IRI = 2.47\ PI_{SOB5} + 0.64$ | |
| | Lower | $IRI = 2.47\ PI_{SOB5} + 0.13$ | |
| SOB6: $\lambda$ = 11.31–22.62 m | Upper | $IRI = 2.14\ PI_{SOB6} + 1.98$ | 0.73 |
| | Average | $IRI = 2.14\ PI_{SOB6} + 0.89$ | |
| | Lower | $IRI = 2.14\ PI_{SOB6} - 0.14$ | |
| DOB4: $\lambda$ = 2.828–11.31 m | Upper | $IRI = 1.85\ PI_{DOB4} + 0.61$ | 0.97 |
| | Average | $IRI = 1.85\ PI_{DOB4} + 0.25$ | |
| | Lower | $IRI = 1.85\ PI_{DOB4} - 0.06$ | |
| DOB5: $\lambda$ = 5.657–22.62 m | Upper | $IRI = 1.77\ PI_{DOB5} + 1.47$ | 0.86 |
| | Average | $IRI = 1.77\ PI_{DOB5} + 0.67$ | |
| | Lower | $IRI = 1.77\ PI_{DOB5} + 0.10$ | |
| DOB6: $\lambda$ = 11.31–45.25 m | Upper | $IRI = 1.49\ PI_{DOB6} + 2.10$ | 0.60 |
| | Average | $IRI = 1.49\ PI_{DOB6} + 0.87$ | |
| | Lower | $IRI = 1.49\ PI_{DOB6} - 0.11$ | |
| TOB2: $\lambda$ = 5.657–45.25 m | Upper | $IRI = 1.43\ PI_{TOB2} + 1.57$ | 0.75 |
| | Average | $IRI = 1.43\ PI_{TOB2} + 0.62$ | |
| | Lower | $IRI = 1.43\ PI_{TOB2} - 0.18$ | |

SOB, DOB and TOB = Single, double and triple octave bandwidths

PI = Calculated profile index between the stated cut-off wavelengths via the Butterworth Filter (Eq. 1) over 100 m pavement sections (m/km)

IRI = International roughness index over 100 m pavement sections (m/km)

At first, the identification of pavement sections with high concentrations of waveband roughness was performed using a colour-coded spread sheet rather than physically plotting thousands of points onto individual templates. This was achieved by mathematically transforming each calculated profile index value (from the raw longitudinal profile) into equivalent IRI values using the appropriate regression equations (i.e. the lower, average and upper confidence limit equations). This established the three relevant boundary points that separated zones 1, 2, 3 and 4 for each associated template. The actual IRI value for each section was then compared to these matching boundary points and categorised into the correct zone. In addition, profile indices that were categorised as zone 1 were also ranked based on the percentage difference between the actual IRI value and the calculated zone 1 boundary point. This permitted a quick identification to the level of waveband roughness concentration present in the pavement. Once all pavement sections were identified, individual 100 m pavement sections were further evaluated in detail. This was typically performed by mapping the profile index versus zone number. An example of this mapping exercise to identify high concentrations of waveband roughness is shown in Fig. 6. In this figure, the detection of waveband roughness concentrations for a 100 m section along the Borung Highway (in north-west Victoria, Australia) is presented. Here, the long waveband roughness concentrations were clearly dominant as wavebands DOB5, SOB6, TOB2 and SOB6 (i.e. wavelengths of 5.657–45.25 m) all recorded zone 1 status on the relevant template.

Upon viewing the "elevation" digital images captured from the vehicle during the road profile survey for the section of road featured in Fig. 6, they did not reveal any evidence of the presence Gilgai relief or long wavelength roughness. It was not until the site was examined using aerial images from Google Earth that the surrounding terrain showed strong signs of the presence of Gilgai relief in the adjacent road reserve. An aerial image from Google Earth of this site has been presented in Fig. 7. Although this image is not very clear, the light and dark patches in the road reserve are distinct and do resemble the mounds and troughs of Gilgai relief respectively. The wavelength of the Gilgai relief at this site was estimated to be between 8 and 12 m, which correlated very well with the high concentrations of waveband roughness detected in the pavement. Surprisingly, evidence of Gilgai relief was only present in the road reserve and not in the adjacent fields. This was most likely due to the regular ploughing of these fields and the continuous break down of the Gilgai structure.

As a result of this image (Fig. 7) being recorded mid-April (Autumn) 2008, the vegetation is relatively green and indicates that a reasonable amount of moisture was present on the site at this time. In contrast, a Google Earth aerial

**Map of Abnormal Concentrations of Waveband Roughness Levels - (Left Wheel Path)**

| | | | Short Wavelength Roughness | | | | | | | | Long Wavelength Roughness | | | | | | | | | | | | | |
|---|---|---|---|---|---|---|---|---|---|---|---|---|---|---|---|---|---|---|---|---|---|---|---|---|
| | | | DOB2 | | SOB3 | | TOB1 | | DOB3 | | SOB4 | | DOB4 | | SOB5 | | DOB5 | | SOB6 | | TOB2 | | DOB6 | |
| | | $\lambda_{Lower}$ | 0.707m | | 1.414m | | 0.707m | | 1.414m | | 2.828m | | 2.828m | | 5.657m | | 5.657m | | 11.31m | | 5.657m | | 11.31m | |
| | | $\lambda_{Upper}$ | 2.828m | | 2.828m | | 5.657m | | 5.657m | | 5.657m | | 11.31m | | 11.31m | | 22.62m | | 22.62m | | 45.25m | | 45.25m | |
| | | $\lambda_{Centre}$ | 1.414m | | 2m | | 2m | | 2.828m | | 4m | | 5.657m | | 8m | | 11.31m | | 16m | | 16m | | 22.62m | |
| | Chainage | Year | Butterworth - MAV | Butterworth - RMS | Butterworth - MAV | Butterworth - RMS | Butterworth - MAV | Butterworth - RMS | Butterworth - MAV | Butterworth - RMS | Butterworth - MAV | Butterworth - RMS | Butterworth - MAV | Butterworth - RMS | Butterworth - MAV | Butterworth - RMS | Butterworth - MAV | Butterworth - RMS | Butterworth - MAV | Butterworth - RMS | Butterworth - MAV | Butterworth - RMS | Butterworth - MAV | Butterworth - RMS |
| Borung Hwy | 126150 m | 1995 | 3 | 3 | 4 | 4 | 3 | 3 | 4 | 4 | 4 | 4 | 4 | 4 | 2 | 3 | 1 | 1 | 1 | 1 | 1 | 1 | 1 | 1 |
| | | 1997 | 3 | 3 | 3 | 4 | 3 | 3 | 4 | 4 | 4 | 4 | 4 | 4 | 3 | 3 | 1 | 1 | 1 | 1 | 1 | 1 | 1 | 1 |
| | | 1999 | 3 | 3 | 3 | 3 | 3 | 3 | 4 | 4 | 4 | 4 | 4 | 4 | 2 | 3 | 1 | 1 | 1 | 1 | 1 | 1 | 1 | 1 |
| | | 2001 | 3 | 3 | 3 | 4 | 3 | 4 | 4 | 4 | 4 | 4 | 3 | 3 | 2 | 2 | 1 | 1 | 1 | 1 | 1 | 1 | 1 | 1 |
| | | 2005 | 4 | 4 | 4 | 4 | 4 | 4 | 4 | 4 | 3 | 3 | 2 | 2 | 1 | 2 | 1 | 1 | 1 | 1 | 1 | 1 | 1 | 1 |
| | | 2007 | 4 | 4 | 4 | 4 | 4 | 4 | 4 | 4 | 4 | 4 | 3 | 3 | 2 | 2 | 1 | 1 | 1 | 1 | 1 | 1 | 1 | 1 |
| | | 2009 | 4 | 4 | 4 | 4 | 4 | 4 | 4 | 4 | 4 | 4 | 3 | 3 | 2 | 2 | 1 | 1 | 1 | 1 | 1 | 1 | 1 | 1 |

| Legend | | |
|---|---|---|
| | Red = Zone 1: Very High Concentrations of Roughness in a Specific Waveband | 1 |
| | Yellow = Zone 2: Moderate to High Concentrations of Roughness in a Specific Waveband | 2 |
| | Green = Zone 3: Low to Moderate Concentrations of Roughness in a Specific Waveband | 3 |
| | Blue = Zone 4: Very Low Concentrations of Roughness in a Specific Waveband | 4 |

**Fig. 6** Mapping of waveband roughness concentrations using Butterworth filter indices—Borung Highway, chainage 126,100–126,200 m, outer wheel path


**Fig. 7** Aerial image of Borung Highway, 126,100–126,200 m that contains evidence of Gilgai relief in the road reserve (Google Earth dated 16th April, 2008)


**Fig. 8** Aerial image of Borung Highway, 126,100–126,200 m that contains no evidence of Gilgai relief in the road reserve (Google Earth dated 31st January, 2014)

image was captured for the same site in the middle of summer (end of January, 2015), which is presented in Fig. 8. Here, the site is much drier and the image shows no visible sign of Gilgai relief present in the road reserve. Thus, Gilgai relief can only be detected using aerial images when enough moisture is present in the soil. This moisture is essential to enable enough visual differentiation between the mounds and troughs. Furthermore, apart from such seasonal moisture variations, the presence of trees, shrubs and long grasses can obstruct the aerial view of the Gilgai relief patterns. Therefore, a mathematical method (as described in this paper) is warranted to accurately and consistently identify Gilgai relief.

In testing these new templates, 198 km of pavement along the Borung and Henty Highways were evaluated. Both of these highways are low-volume, sealed, two lane, flexible, rural highway pavements located in north-west Victoria, Australia. The majority of these pavement sections are located in areas of highly expansive clay geology (i.e. grey cracking clays), which were expected to reveal a greater number of pavement sections with high concentrations of long wavelength roughness (i.e. evidence of Gilgai relief). The frequency and distribution of the long waveband roughness concentrations detected for the Henty Highway is presented in Table 2. In this table, a value of 2 % is considered to represent a normal or the expected concentration of roughness detection as the upper and lower confidence limits of the templates were based on 98 % limits. Hence, the concentration of roughness in waveband SOB4 appears to be normal as the detection percentage varies between 1.62 and 2.56 %. However, the frequency of roughness concentrations in wavebands DOB4, SOB5, DOB5 and SOB6 were significantly higher. The greatest frequency of 10.8 % occurred at wavebands SOB5 and DOB5, which suggests that the frequency of high long wavelength concentrations along the Henty Highway was over five times that of a normal pavement. Furthermore, the general increase in detection frequency noted from 1997 to 2009 suggests that the long wavelength component of the roughness is increasing at a rate greater than the IRI.

## Conclusions

This paper has presented a new series of templates to identify pavement sections that contain high concentrations of specific waveband roughness, especially for the longer wavelengths. These templates were developed from over six hundred kilometres of road profile data and were tested using nearly two hundred kilometres of pavement. Within the test pavements, many sections were successfully identified and shown to be experiencing distress in the longer wavelengths; largely due to Gilgai relief generated distress.

One of the significant benefits of these new templates is that the influence of Gilgai relief can now be detected and quantified mathematically. This is expected to replace the unreliable visual method of detecting Gilgai relief by using

**Table 2** Frequency of detected long wavelength roughness concentrations, Henty Highway, based on Butterworth (MAV) templates, Inner (right) wheel path [26, Chpt 6]

| Profile index: Butterworth (MAV)—inner wheel path | | | | | | | |
|---|---|---|---|---|---|---|---|
| Waveband<br>Centre Wavelength | SOB4<br>4 m | DOB4<br>5.66 m | SOB5<br>8 m | DOB5<br>11.3 m | SOB6<br>16 m | TOB2<br>16 m | DOB6<br>22.6 m |
| Concentrations detected of long wavelength roughness | | | | | | | |
| 1997 | | | | | | | |
| No. | 19 | 47 | 79 | 88 | 64 | 31 | 19 |
| % | 1.62 | 4.01 | 6.75 | 7.52 | 5.47 | 2.65 | 1.62 |
| 1999 | | | | | | | |
| No. | 21 | 53 | 104 | 107 | 73 | 35 | 16 |
| % | 1.79 | 4.53 | 8.88 | 9.14 | 6.23 | 2.99 | 1.37 |
| 2001 | | | | | | | |
| No. | 26 | 51 | 93 | 93 | 70 | 34 | 24 |
| % | 2.21 | 4.34 | 7.92 | 7.91 | 5.96 | 2.89 | 2.04 |
| 2005 | | | | | | | |
| No. | 17 | 63 | 126 | 126 | 97 | 61 | 42 |
| % | 1.45 | 5.36 | 10.8 | 10.8 | 8.28 | 5.20 | 3.58 |
| 2007 | | | | | | | |
| No. | 21 | 69 | 106 | 126 | 91 | 61 | 45 |
| % | 1.79 | 5.87 | 9.03 | 10.8 | 7.75 | 5.20 | 3.83 |
| 2009 | | | | | | | |
| No. | 30 | 67 | 116 | 121 | 91 | 72 | 52 |
| % | 2.56 | 5.71 | 9.89 | 10.3 | 7.75 | 6.14 | 4.43 |

aerial images. Aerial images cannot always detect Gilgai relief due to the Gilgai often being obstructed by trees, shrubs and long grasses. Furthermore, Gilgai relief is difficult to detect visually during dry periods where moisture levels in the soil are so low that no differentiation is possible between the mound and trough features.

In detecting long wavelength roughness derived from Gilgai relief, it was found that the Butterworth (MAV) based profile index templates (presented in Table 1) performed the best. The second best was the Butterworth (RMS) profile index templates followed by the PSD of profile slope based templates.

The significance of these new templates is that they are expected to provide Road Engineers with a better understanding of the roughness distribution within the pavement as well as the identification of critical wavebands responsible for pavement deterioration. In the future, waveband roughness progression rates should be calculated to provide an even greater understanding to the deterioration process of a pavement. Consequently, this should lead to better maintenance and rehabilitation decisions being made in the future.

**Acknowledgments** The authors would like to thank Mr. Ian Cossens from the Pavement Asset Management Group, VicRoads, who spent much time explaining the State Road Referencing System as well as assisting with the extraction of maintenance records for the test sites. I also acknowledge and appreciate VicRoads for purchasing the required raw longitudinal road profiles measured during the 2007 survey, which was ultimately used to develop the templates presented in this paper.

## References

1. Richards BG (1968) The role of environment in flexible pavement design. Civil Engineering Transactions, The Institution of Engineers, Australia, pp 197–205
2. Richards BG, Peter P, Emerson WW (1983) The effects of vegetation on the swelling and shrinking of soils in Australia. Geotechnique 33(2):129–139
3. Barry IM (1984) The influence of shrubs and trees on pavement loss of shape. VicRoads technical report, VicRoads, Australia, pp 1–27
4. Jameson GW (1986) Trees and pavement shape loss. In: Proceedings of the 13th Australian road research conference, part 4: pavements and construction, Australia, pp 93–106
5. Lopes D, Osman NY (2010) Changes of Thornthwaite's total moisture indices in Victoria from 1948–2007 and the effect of seasonal foundation movements. Aust Geomech 45(1):37–48
6. Luo R, Prozzi JA (2011) Development of longitudinal cracks on pavement over shrinking expansive subgrade. Road Mater Pavement Des 11(4):807–832
7. Velasco MO, Lytton RL (1981) Pavement roughness on expansive clays, TRR790, Washington, DC, pp 78–87

8. Lytton RL, Boggess RL, Spotts JW (1976) Characteristics of expansive soil roughness of pavements, TRR568, Washington, DC, pp 9–23
9. Aitchison GD (1953) The mechanics of gilgai formation. In: Proceedings of the first Australian conference on soil science, vol 2, section 6, paper no. 25, Adelaide, Australia, pp 1–3
10. Beckman GG, Hubble GD, Thompson CH (1970) Gilgai forms, distribution and soil relationships in north-eastern Australia, presented at symposium on soils and earth structures in arid climates, paper no. 2898, May 21–22, The Institution of Engineers, Adelaide, Australia, pp 116–121
11. Bartelli LJ, McCormack DE (1976) Morphology and pedologic classification of swelling soils, TRR568, Washington, DC, pp 1–8
12. Maxwell B (1994) Influence of horizontal stresses on gilgai landforms. J Geotech Eng 120(8):1437–1443
13. Hallwsorth EG (1968) A handbook of Australian soils: X the gilgai phenomenon. Rellim Technical Publications, South Australia, pp 415–423
14. Smith RL (1993) Estimating soil movements in new areas. Presented at australian geomechanics society seminar: extending the code beyond residential slabs and footings, Victoria Branch, Melbourne, Australia, pp 1–6
15. Kassiff G, Holland JE (1966) The expansive properties of Dooen clays as applied to buried pipes. Civ Eng Trans 8(2):133–142
16. Blackburn G, Sleeman JR, Scharpenseel HW (1979) Radiocarbon measurements and soil micromorphology as guides to the formation of gilgai at Kaniva, Victoria. Aust J Soil Res 17:1–15
17. Knight MJ (1980) Structural analysis and mechanical origins of gilgai at Boorook, Victoria, Australia. Geoderma 23(4):245–283
18. Sayers MW, Gillespie TD, Queiroz CAV (1986) The international road roughness experiment: a basis for establishing a standard scale for road roughness measurements. Journal of the Transportation Research Board, Transportation Research Record No. 1084, Transportation Research Board of the National Academies, Washington, DC, pp 76–85
19. Sayers MW, Gillespie TD, Queiroz CA (1986) The international road roughness experiment: establishing correlation and a calibration standard for measurements. World Bank technical paper number 45, The World Bank, Washington, DC, USA
20. Sayers MW (1995) On the calculation of international roughness index from longitudinal road profile. Journal of the Transportation Research Board, Transportation Research Record No. 1501, National Research Council, Washington, DC, USA, pp 1–12
21. ASTM E1926 (1998) E1926 98: standard practice for computing international roughness index of roads from longitudinal profile measurements. ASTM International, Leyden
22. Sayers MW, Karamihas SM (1998) The little book of profiling: basic information about measuring and interpreting road profiles. The University of Michigan Transportation Research Institute, Ann Arbor
23. Hassan R, Evans R (2013) Road roughness characteristics in car and truck wheel tracks. Int J Pavement Eng 14(8):736–745
24. Butterworth S (1930) On the theory of filter amplifiers. Exp Wirel Wirel Eng 7:536–541
25. UMTRI (1997) RoadRuf: software for analysing road profiles. University of Michigan Transportation Research Institute, Ann Arbor
26. Evans RP (2013) Synchronisation of road profile data and the assessment of road roughness using waveband analysis. PhD Dissertation, Swinburne University of Technology, Melbourne, Australia
27. Mann A, McManus KJ, Evans RP (1998) The use of power spectral density analysis to determine deterioration modes in pavement structures. In: Proceedings of the 9th REAAA conference, Wellington, New Zealand, vol 2, pp 263–268
28. ISO 8608 (1995) ISO 8608 mechanical vibration—road surface profiles—reporting of measured data. International Organization of Standardization, Geneva